Distortion of a Spherical Gaseous Interface Accelerated by a Plane Shock Wave

Guillaume Layes, Georges Jourdan, and Lazhar Houas*

Polytech'Marseille, Département Mécanique Énergétique, IUSTIUMR CNRS 6595, Technopôle de Château Gombert, 5, rue Enrico Fermi, 13013 Marseille, France

(Received 6 May 2003; published 24 October 2003)

The evolution of a spherical gaseous interface accelerated by a plane weak shock wave has been investigated in a square cross section shock tube via a multiple exposure shadowgraph diagnostic. Different gaseous bubbles, i.e., helium, nitrogen, and krypton, were introduced in air at atmospheric pressure in order to study the Richtmyer-Meshkov instability in the spherical geometry for negative, close to zero, and positive initial density jumps across the interface. We show that the bubble distortion is strongly different for the three cases and we present the experimental velocity and volume of the developed vortical structures. We prove that at late times the bubble velocities reach constant values which are in good agreement with previous calculations. Finally, we point out that, in our flow conditions, the gaseous bubble motion and shape are mainly influenced by vorticity and aerodynamic forces.

DOI: 10.1103/PhysRevLett.91.174502 PACS numbers: 47.40.Nm, 47.20.Ma

The instability mechanism which appears at a spherical interface between two fluids of different density accelerated by a shock wave is both complex and of fundamental interest (turbulence generation and mixing intensification). It is referred to as the Richtmyer-Meshkov instability (RMI) [1,2]. Our research deals with the validation of inertial confinement fusion (ICF) computer simulations. Thus, the aim of the present work is to experimentally investigate the interaction of a plane shock wave with a single discrete spherical gaseous inhomogeneity in order to better understand the RMI process in this geometry and its effect on the generated turbulent mixing as well as on the velocity and volume evolutions of the bubble. The interaction of a shock wave with a fluid inhomogeneity alters its morphology, sets it in motion, and creates vorticity. Furthermore, as it has been shown in the previous work of Haas and Sturtevant [3], the bubble deformation is completely different regarding the cases where the shock wave passes from the heavy gas to the light one or from the light to the heavy one. Unfortunately, in that referenced work, only average velocities had been determined (only one shot per run) and no information on the volume was presented. The experiments undertaken in the present study are based on multiple exposure shadowgraph frames taken during the same run for different times via a high speed photography system. As in the previous work of Jourdan *et al.* [4], the main cases have been studied, when the shock wave passes from a main gas (air) to an inhomogeneity filled with a lighter (He), a heavier (Kr), or of close density (N_2) gas.

The experiments have been performed in our 8 cm by 8 cm square cross section shock tube previously described by Devals *et al.* [5]. Its total length is 3.75 m and the high pressure chamber is 0.75 m long. It is equipped with a high speed rotating camera shadowgraph system (High Speed Photo-System Company, Wedel, Germany) synchronized with a stroboscopic Nanolite flash lamp (one flash each 70 μs). This device allows us to reconstruct the experimental history of the gaseous inhomogeneity motion and deformation by processing the consecutive frames obtained during one experiment (100 frames/run, i.e., 7 ms of total observation time). The total observation zone is of 8 cm by 30 cm. The He, N_2, or Kr bubbles are created with a $\frac{1}{3}$ shampoo, $\frac{1}{3}$ water, and $\frac{1}{3}$ glycerin handmade mixture carefully deposited on a support centered in the test section of the shock tube. It consists of a spherical curved small brass cup (6 mm diameter, 1 mm pierced) soldered to a 2 cm long vertical brass tube (2 mm external and 1 mm internal diameter, respectively). It is connected to an airtight system linked to a gaseous tank via a pressure reducer. In all experiments, the gas initially surrounding the bubble is air at atmospheric pressure. The incident shock wave Mach number is less than 1.25. The bubble size has been optimized to be of about 4 cm diameter so that the influence of wall effects on the process can be neglected.

Figures 1(a)–1(c) illustrate the gaseous bubble deformations for the heavy/light (H/L), close density (CD), and light/heavy (L/H) experimental configurations, respectively. In all frames, the incident shock wave is moving from right to left as well as the deformed bubble and main flow. Frames 0 of Figs. 1(a)–1(c) give the initial conditions for each corresponding experiment. As the incident shock wave is confronted to a spherical inhomogeneity (spherical reflection) in a different media (spherical transmission with velocity modification), it generates an incident shock moving in air surrounding the bubble, a reflected one moving back in air, and a transmitted one within the bubble. Furthermore, if density and pressure gradients are noncollinear, vorticity is generated. Note that, in all cases, a small scale instability occurs on the surface of the bubble, probably due to the nonuniformity of the soap membrane.

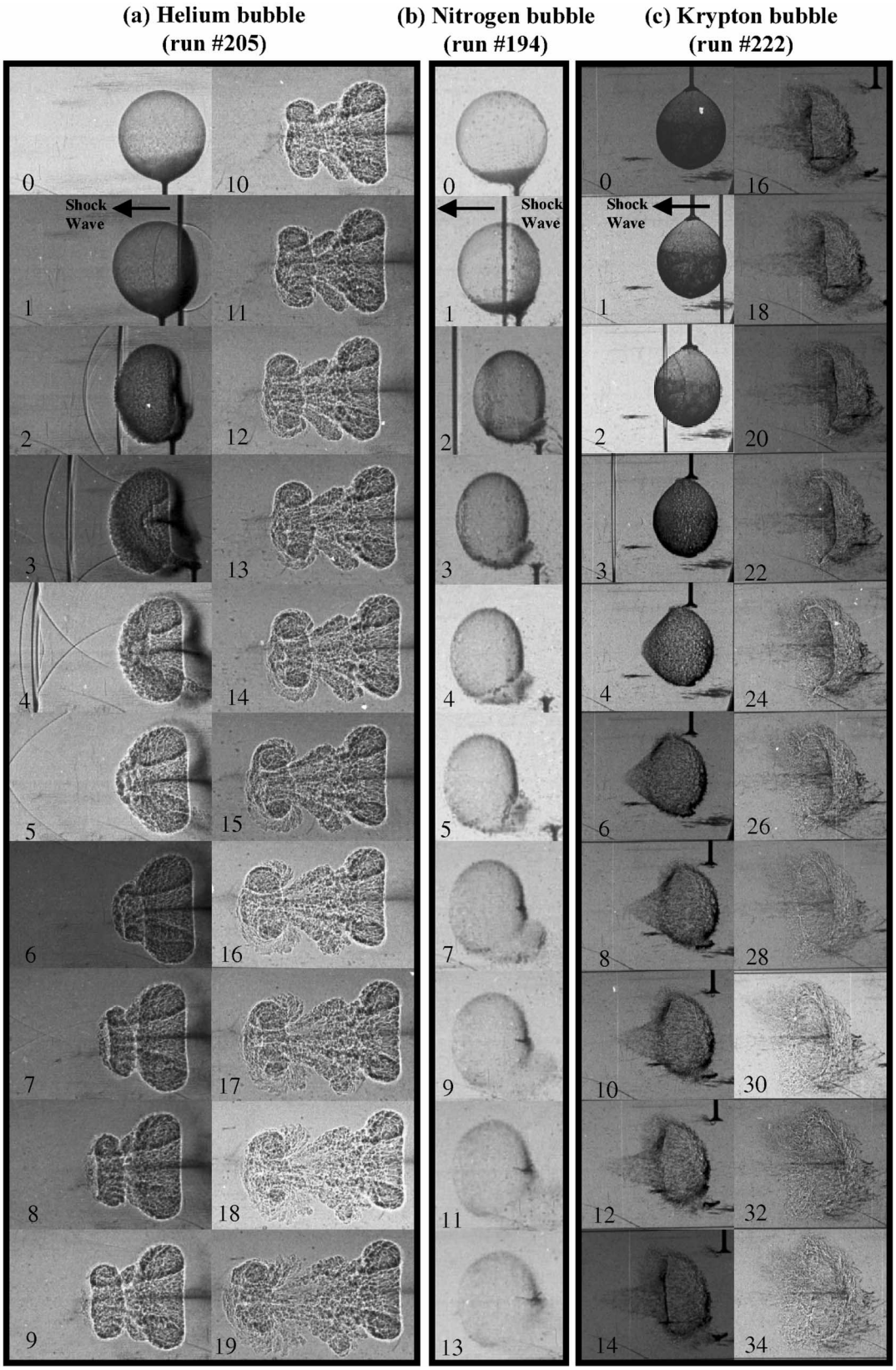

FIG. 1. Shadowgraph frames of the interaction between a shock wave moving in air and a gaseous bubble for (a) the H/L case (4.3 cm diameter He bubble), (b) the CD case (3.7 cm diameter N_2 bubble), and (c) the L/H case (3.9 cm vertical and 3.6 cm horizontal diameters Kr bubble). The incident shock wave is moving from right to left and two consecutive frames are separated by 70 μs. The initial time on frame 0 is (a) $t = 45$ μs, (b) $t = 60$ μs, and (c) $t = 25$ μs before interaction. The image size is (a) 9.9 cm $\times$ 6.6 cm, (b) 6.6 cm $\times$ 6.6 cm, and (c) 7.4 cm $\times$ 6.6 cm.

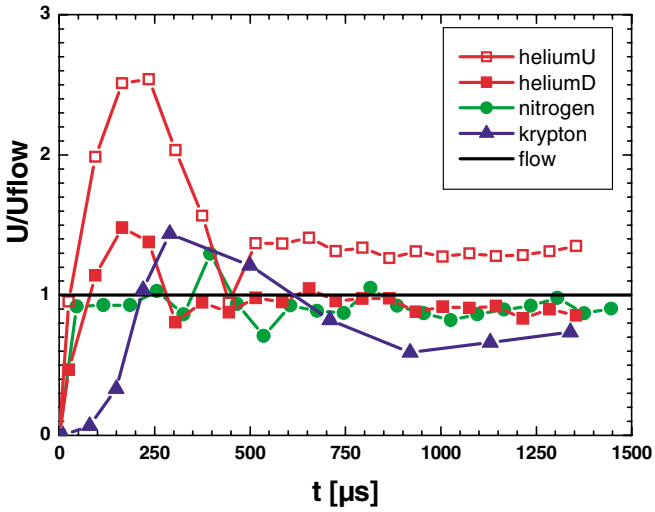

FIG. 2 (color online). Evolution of the normalized velocity for He (upstream and downstream rings), N_2, and Kr bubbles moving in air.

Frame 1 of Fig. 1(a) shows the incident shock wave interaction with the He bubble. Indeed, due to a high difference in speed of sound between air (342 m/s) and He (1010 m/s), the curved transmitted shock wave within the He gaseous bubble moves faster and is weakly observable ahead of the incident one. The curved reflected shock wave (on the soap interface) moving back in air is clearly visible on the right side of the bubble. In frame 2, the He curved transmitted shock wave, now moving in air, is followed by the incident one. It is not seen on the zoomed frame, but they completely converge after 420 μs (which corresponds to frame 8). Concerning the inhomogeneity deformation, as it is less dense than the surrounding media, the main flow velocity behind the incident shock wave acts like a piston on the bubble. Thus, the downstream interface (air/He) reaches a higher velocity than the upstream one (He/air). It results in the bubble reversal (frames 2 to 5). Then (in frame 6), the air passes through the He bubble and what happens later looks like air passing through a divergent passage. This process captures He and a second upstream ring appears. Moreover, as deduced hereafter from the velocity measurements, vorticity concentrates on this ring. It is useful to be precise herein that the downstream interface generates the upstream ring while the upstream interface gives the downstream ring. The consequence is that vorticity increases the upstream ring velocity to a higher value than that of the main flow, while the downstream ring reaches a velocity close to this last one. Then, the rings move away from each other until the link between them is broken and then the ring motions become independent.

Figure 1(b) shows the development process of a gaseous bubble (N_2) of density close to that of the surrounding media (air). As expected, no particular deformation is observed except the weak compression due to the shock and the perturbations generated by the bubble support.

Figure 1(c) presents the case of a Kr bubble in air (L/H). The main observation is that the deformation process is physically completely different than the H/L case. Regarding the different speed sound velocities, the reflected shock wave in air can be seen in frame 1, while the transmitted one in Kr is observable behind the incident shock wave in frame 2. Concerning the heavy gas bubble deformation, we think that the shock wave passage generates a flow surrounding the bubble which acts as an obstacle. Then a drag appears on the left side of it, and by a clockwise rotation of $\pi/2$, it looks like a water droplet falling down in air (frames 4 to 6). Next, the bubble is symmetrically and three dimensionally dug on its upstream face and a ring appears on it, too, as air moving round the bubble rolls up beside it. Finally, its shape looks like a medusa and, in the last frames, more like an umbrella. In the same way, vorticity is initiated during the interaction and develops. It concentrates on the ring created by the aerodynamic forces and slows its velocity. To conclude in Fig. 1, we believe that in both H/L and L/H deformation processes, aerodynamic forces as well as vorticity govern the shape and the motion of the bubble.

Figure 2 represents the bubble interface velocity normalized by the main flow speed for the three cases. For the H/L case, the velocity of the He upstream vortex ring and the He downstream ring have been plotted. For the CD and L/H cases only the velocity of the upstream interface has been represented, as the bubble stays in one piece. Note that in the L/H case, this velocity corresponds to that of the vortical structure. In all cases, the range of errors on velocity values is of about 10% to 20% and decreases with time as velocity stabilizes. The first interesting case is the similar density one. While there is

TABLE I. Comparison of the present experimental work results with previous numerical ones. At* is the postshock Atwood number, M is the shock wave Mach number, U_{flow} is the main flow velocity, U_{up} is the upstream bubble interface velocity, and U_{down} is the downstream bubble interface velocity.

Bubble gas	At*	M	U_{flow} [m/s]	Experiments $U_{\text{up}}/U_{\text{down}}$ [m/s]	Picone and Boris (Ref. [6]) $U_{\text{up}}/U_{\text{down}}$ [m/s]	Yang *et al.* (Ref. [7]) $U_{\text{up}}/U_{\text{down}}$ [m/s]
Helium	−0.78	1.24	118	110/155	118/176	118/181
Nitrogen	≈ 0	1.18	91	82/85	...	...
Krypton	0.48	1.10	52	42/35	52/41	52/41

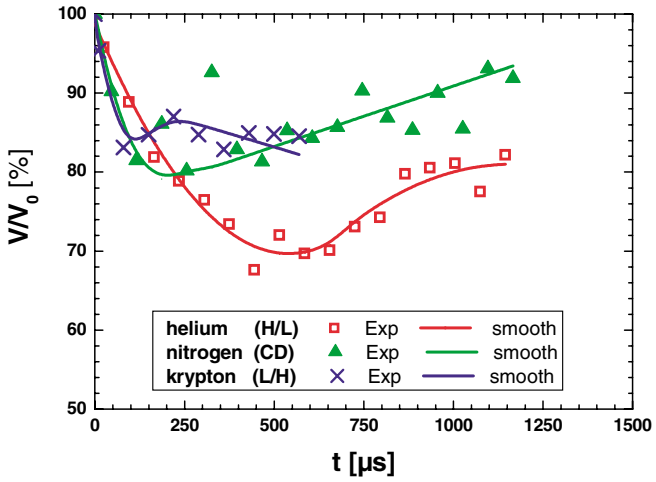

FIG. 3 (color online). Evolution of the normalized volume for He, N_2, and Kr bubbles moving in air.

no density gradient, there will be no vorticity generation and the motion of the bubble is only the result of the impulse provided by the shock moving in air. We observe then that the inhomogeneity nearly reaches the main flow velocity. Concerning He and Kr bubbles, numerical simulations [6,7] have shown that, on the one hand, vorticity will modify the velocity of the inhomogeneity compared to that of the flow. It has been found that for a lighter inhomogeneity, the velocity will be higher than that of the flow, whereas it will be smaller for a heavy one. On the other hand, both models have also predicted that for the H/L case, vorticity will concentrate on the upstream ring. Both the results presented in Fig. 2 and the values given in Table I are in good agreement with these lightly overestimated predictions. First, we can see that the upstream ring of the H/L case goes faster than the flow. This confirms that there is vorticity in it and that, as predicted, it increases the ring velocity. Moreover, the downstream ring had a velocity similar to that of the flow so there is no or few vorticity in it, and for the L/H case, the vortex has a smaller speed than the flow. This means that, here, vorticity slows down the inhomogeneity.

Figure 3 gives the evolution of the bubble volume normalized by the initial one for the three tested cases. As the visualization method gives only 2D information, some assumptions have to be made to determine the volume. First, we suppose that the shadowgraph frames represent the median section of the bubble. Second, we assume that the gaseous inhomogeneities admit a symmetrical axis (horizontal for H/L and CD cases, vertical for the L/H case). Last, when necessary, the global volume is cut in smaller simplest ones so that common geometric volume formulas can be applied. However, volume is still hard to be deduced (particularly at late times and for the L/H case) and error bars are estimated to be of about $\pm 10\%$. Nevertheless, as seen in Fig. 3, for all cases, we observe that a compression of the inhomogeneity volume follows the shock wave passage. For the CD case, as explained above, while no vorticity is generated, no deformation appears. Only a compression due to the shock wave passage is observable and followed by a linear volume increase. For the two other cases, as there is also a deformation due to vorticity, to quantify the effect of each is difficult. For the H/L case, the compression and the reversal of the bubble reduce the bubble volume until a minimum value is reached as the downstream interface meets the upstream one. Next, the second ring (the upstream one) appears and the global volume increases as can be seen in the frames of Fig. 1(a). However, for the L/H case, as time increases it becomes harder to fit the shape of the bubble and to estimate its volume, and then to give any conclusion. Finally, note that for the H/L and L/H cases, the distorted bubbles contain a mixing of the two gases. It is this volume that we have calculated. Nevertheless, it would be interesting to seed one of the two gases in order to better understand their distribution in the mixing.

In summary, an experimental investigation of the evolution of a spherical gaseous inhomogeneity accelerated by a planar shock wave has been undertaken for negative, close to zero, and positive initial density jumps across the interface. We have shown that, for our flow conditions, vorticity as well as aerodynamic forces mainly govern the phenomenon. The shock wave compression phase is well observable on the frames as well as on volume curve. Furthermore, we point out that, at last times, the bubble velocities reach a constant value, as predicted by previous theoretical and numerical works, with a good agreement. It has been also found that a lighter inhomogeneity vortex reaches a higher velocity than that of the main flow, whereas it is smaller for a heavy one. Finally, as a bubble is a zoom of what happens at the interface of ICF experiments, this work may be useful for better understanding of RMI and modeling issues of turbulent mixing zone.

This work was supported by the CEA-DAM, Bruyères-le-Châtel (France) under Contract No. 4600048096/P6H29. The authors thank R. Saurel, D. Souffland, and F. Renaud for valuable discussions.

*Electronic address: Lazhar.Houas@polytech.univ-mrs.fr

[1] R. Richtmyer, Commun. Pure Appl. Math. **13**, 297 (1960).
[2] E. Meshkov, Fluid Dyn. **4**, 101 (1969).
[3] J. Haas and B. Sturtevant, J. Fluid Mech. **181**, 41 (1987).
[4] G. Jourdan, L. Houas, and M. Billiotte, Phys. Rev. Lett. **78**, 452 (1997).
[5] C. Devals, G. Jourdan, J. Estivalezes, E. Meshkov, and L. Houas, Shock Waves **12**, 325 (2003).
[6] J. Picone and J. Boris, J. Fluid Mech. **189**, 23 (1988).
[7] J. Yang, T. Kubota, and E. Zuboski, J. Fluid Mech. **258**, 217 (1994).